PAPER

The mechanically induced structural disorder in barium hexaferrite, BaFe$_{12}$O$_{19}$, and its impact on magnetism

V. Šepelák,†*[ab] M. Myndyk,[c] R. Witte,[a] J. Röder,[d] D. Menzel,[e] R. H. Schuster,[bf] H. Hahn,[a] P. Heitjans[bg] and K.-D. Becker[bh]

The response of the structure of the M-type barium hexaferrite (BaFe$_{12}$O$_{19}$) to mechanical action through high-energy milling and its impact on the magnetic behaviour of the ferrite are investigated. Due to the ability of the ^{57}Fe Mössbauer spectroscopic technique to probe the environment of the Fe nuclei, a valuable insight on a local atomic scale into the mechanically induced changes in the hexagonal structure of the material is obtained. It is revealed that the milling of BaFe$_{12}$O$_{19}$ results in the deformation of its constituent polyhedra (FeO$_6$ octahedra, FeO$_4$ tetrahedra and FeO$_5$ triangular bi-pyramids) as well as in the mechanically triggered transition of the Fe^{3+} cations from the regular 12k octahedral sites into the interstitial positions provided by the magnetoplumbite structure. The response of the hexaferrite to the mechanical treatment is found to be accompanied by the formation of a non-uniform nanostructure consisting of an ordered crystallite surrounded/separated by a structurally disordered surface shell/interface region. The distorted polyhedra and the non-equilibrium cation distribution are found to be confined to the amorphous near-surface layers of the ferrite nanoparticles with the thickness extending up to about 2

^{a}*Institute of Nanotechnology, Karlsruhe Institute of Technology (KIT), Hermann-von-Helmholtz-Platz 1, D-76344 Eggenstein-Leopoldshafen, Germany. E-mail: vladimir.sepelak@kit.edu; Fax: +49-721-60826368; Tel: +49-721-60828929*

^{b}*Center for Solid State Chemistry and New Materials, Leibniz University Hannover, Callinstr. 3-3a, D-30167 Hannover, Germany*

^{c}*Department of Inorganic Chemistry, Dresden University of Technology, Mommsenstr. 6, D-01062 Dresden, Germany*

^{d}*Physics Department, European Council for Nuclear Research (CERN), CH-1211 Geneva 23, Switzerland*

^{e}*Institute of Condensed Matter Physics, Braunschweig University of Technology, Mendelssohnstr. 3, D-38106 Braunschweig, Germany*

^{f}*German Institute of Rubber Technology (DIK), Eupener Str. 33, D-30519 Hannover, Germany*

^{g}*Institute of Physical Chemistry and Electrochemistry, Leibniz University Hannover, Callinstr. 3-3a, D-30167 Hannover, Germany*

^{h}*Institute of Physical and Theoretical Chemistry, Braunschweig University of Technology, Hans-Sommer-Str. 10, D-38106 Braunschweig, Germany*

† On leave from the Slovak Academy of Sciences, Košice, Slovakia.
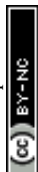
nm. The information on the mechanically induced short-range structural disorder in $BaFe_{12}O_{19}$ is complemented by an investigation of its magnetic behaviour on a macroscopic scale. It is demonstrated that the milled ferrite nanoparticles exhibit a pure superparamagnetism at room temperature. As a consequence of the far-from-equilibrium structural disorder in the surface shell of the nanoparticles, the mechanically treated $BaFe_{12}O_{19}$ exhibits a reduced magnetization and an enhanced coercivity.

Introduction

Mechanically induced chemistry (the so-called mechanochemistry) as a branch of chemistry, being concerned with the chemical and physical transformations of solids induced by mechanical action, continues to be of high importance.[1] Among the inorganic materials susceptible to mechanical action, oxides exhibit a wide range of responses.[2] In particular, complex oxides possessing more than one cation sublattice, such as spinels, olivines and mullites (with two cation sub-lattices), have been considered as convenient model systems for the investigation of mechanically induced processes in ionic systems, because of their structural flexibility providing a wide range of physical and chemical behaviours.[3] Despite their deceptively simple structure, many oxides exhibit complex disordering phenomena under the influence of mechanical action. These involve, for example, (i) the mechanically induced redistribution of cations over non-equivalent cation sublattices provided by a complex oxide structure, (ii) the formation of canted spin arrangements in the case of magnetic compounds, (iii) the changes in the geometry of constitutive polyhedra, and (iv) the mechanically triggered formation of defective cation centers with an unsaturated oxygen coordination.[3,4]

Although there is a surge of investigations in the field of mechanochemistry of oxides, studies on the mechanically induced response of complex oxides possessing more than two cation sublattices, such as M-type barium hexaferrite, $BaFe_{12}O_{19}$ (with five cation sublattices), are very scarce in the literature.[5,6] As a result of its specific magnetic properties, $BaFe_{12}O_{19}$ is widely used in permanent magnets, magnetic recording media and microwave applications. Its derivatives are currently magnetic materials with great scientific and technological interests due to their relatively high Curie temperature, high coercive force and high magnetic anisotropy field as well as their excellent chemical stability and corrosion resistivity. Recently, multiferroic properties have been reported for $BaFe_{12}O_{19}$ ceramics.[7] In this article, for the first time, detailed information is obtained on the response of the local (short-range) structure of $BaFe_{12}O_{19}$ to mechanical action through high-energy milling. In addition to ^{57}Fe Mössbauer spectroscopy, the evolution of the mechanically induced structural disorder as well as the morphology and macroscopic magnetic behaviour of the ferrite were monitored with comprehensive techniques including X-ray diffraction (XRD), high-resolution transmission electron microscopy (TEM), and superconducting quantum interference device (SQUID) magnetometry.

Experimental

M-type $BaFe_{12}O_{19}$, which was used as the starting material for subsequent mechanochemical treatment, was synthesized using a chemically reliable
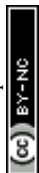
co-precipitation route.[8] The precursor materials of barium and iron chlorides (99.9% purity; Merck, Darmstadt, Germany) were dissolved in deionized water, and subsequently solutions of Na_2CO_3 and NaOH were added to achieve pH = 6. The precipitated precursor was sintered at 1173 K to obtain bulk $BaFe_{12}O_{19}$ (which is further referred to as the non-treated material). Fig. 1 shows the morphology of the as-prepared bulk $BaFe_{12}O_{19}$ powder, which served as a reference sample in the present study. The particles of the co-precipitated ferrite were found to be uniform in shape; the majority of them are hexagonal platelet crystals. Whereas the thickness of the ferrite platelets is in the 20 – 100 nm range, their length ranges from 300 to 400 nm. The corresponding selected area electron diffraction (SAED) pattern of the ferrite (Fig. 1b) is dominated by the discrete diffraction spots originating from the well crystalline hexagonal platelets.

10 grams of the bulk material were mechanically treated for various times t_m (up to 8 h) in a high-energy planetary mill Pulverisette 6 (Fritsch, Idar-Oberstein, Germany) at room temperature. A grinding chamber (250 cm^3 in volume) and balls (10 mm in diameter) made of tungsten carbide were used. The ball-to-powder weight ratio was 20 : 1. The milling experiments were performed in air at 600 rpm.

The XRD patterns were measured using a PW 1820 X-ray diffractometer (Philips, Netherlands), operating in Bragg configuration and using Cu Kα radiation (λ = 1.54056 Å). The XRD scans were collected from 10° to 80° (2Θ), using a step of 0.02° and a data collection time of 5 s. The JCPDS PDF database[9] was utilized for phase identification using the STOE software. The hexagonal structure of $BaFe_{12}O_{19}$ was visualized using the Diamond program[10] and Java Structure Viewer software.[11]

The ^{57}Fe Mössbauer spectra were taken at 293 K in transmission geometry using a $^{57}Co/Rh$ γ-ray source. Recoil spectral analysis software[12] was used for the quantitative evaluation of the Mössbauer spectra. The velocity scale of the spectra was calibrated relative to ^{57}Fe in Rh.

The morphology of the powders was studied using a combined field-emission (scanning) transmission electron microscope (S)TEM (JEOL JEM-2100F) with a high-resolution pole piece that provides a point resolution better than 0.19 nm at 200 kV. Prior to the TEM investigations, the powders were crushed in a mortar, dispersed in ethanol, and fixed on a copper-supported carbon grid.

The magnetic measurements were performed using a SQUID magnetometer (Quantum Design MPMS-5S, USA). The samples were filled in a small container
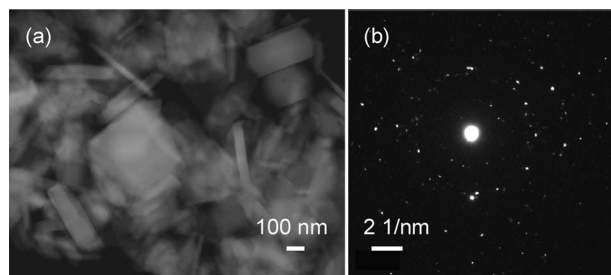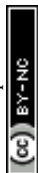

Fig. 1 (a) The electron microscopy image and (b) the corresponding SAED pattern illustrating the presence of hexagonal platelet crystals in the co-precipitated $BaFe_{12}O_{19}$.

made of polyvinyl chloride, whose diamagnetic moment was subtracted from the measured magnetization values. Magnetic hysteresis loops were recorded at 5 K in external magnetic fields from 0 to ± 5 T.

Results and discussion

Prior to any characterization of the structural disorder and functional properties of the mechanically treated $BaFe_{12}O_{19}$, the atomic configuration of the non-treated bulk material has to be known. An effective way to do this is by means of nuclear spectroscopic techniques such as ^{57}Fe Mössbauer spectroscopy, which makes possible observations on a local atomic scale. This spectroscopic method has been proven to be well suited for the investigation of the charge state, the local coordination, and the magnetic state of iron ions in various ferrites.[13] Fig. 2 illustrates the room temperature ^{57}Fe Mössbauer spectrum of the $BaFe_{12}O_{19}$ standard sample. As can be seen, the spectrum of the material is well-fitted by a superposition of five magnetically split spectral components (sextets) indicating the presence of five different atomic environments around the iron nuclei. Three sextets with isomer shift IS > 0.19 mm s^{-1} (see Table 1) correspond to octahedrally coordinated ferric (Fe^{3+}) ions in the $4f_2$, 12k and 2a crystal sites of the hexagonal structure of the ferrite.[14] The spectral component with the lowest value of IS ($\sim$ 0.14 mm s^{-1}) is typical for Fe^{3+} cations in tetrahedral ($4f_1$) coordination of oxygen anions.[15] The sextet with a relatively large quadrupole splitting (QS $\sim$ 1.1 mm/s), indicating the presence of a large electric field gradient acting on the iron nuclei, corresponds to Fe^{3+} ions in the trigonal bi-pyramidal (2b) sites of $BaFe_{12}O_{19}$. The Mössbauer parameters resulting from the least-squares fitting of the spectrum of bulk $BaFe_{12}O_{19}$ (Table 1) are in reasonable agreement with those determined in previous work.[14] From the relative intensities of the sextets, the number of Fe^{3+} cations located on the $4f_2$, 12k, 2a, $4f_1$ and 2b sublattices was calculated to be 2, 6, 1, 2 and 1 per formula unit (f.u.) of $BaFe_{12}O_{19}$, respectively. Based on the present Mössbauer results, the structural formula of $BaFe_{12}O_{19}$, emphasizing the site occupancy at the atomic level, may be written as Ba
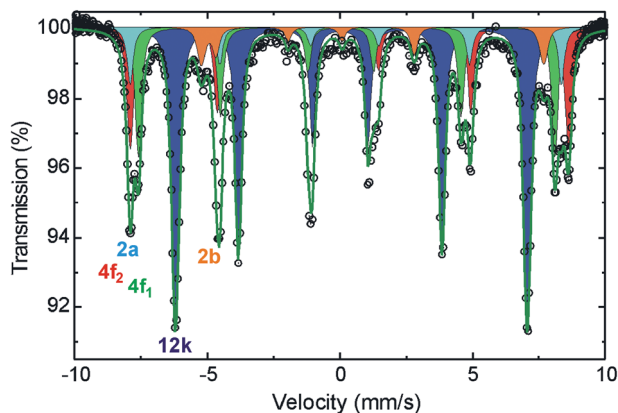

Fig. 2 The room temperature ^{57}Fe Mössbauer spectrum of the standard $BaFe_{12}O_{19}$ sample. The red, blue, cyan, green and orange colours denote the subspectra corresponding to the Fe^{3+} cations in the 4f2, 12k, 2a, 4f1, and 2b sublattices, respectively.
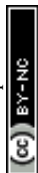
Table 1 The parameters obtained by fitting the room temperature ^{57}Fe Mössbauer spectrum of polycrystalline $BaFe_{12}O_{19}$[a]

Site	Coordination of Fe^{3+} ions	IS (mm s^{-1})	QS (mm s^{-1})	H (T)	Number of Fe^{3+} ions per f.u.
$4f_2$	Octahedral	0.252(7)	0.102(8)	51.21(8)	2
12k	Octahedral	0.218(1)	0.210(1)	41.10(1)	6
2a	Octahedral	0.196(2)	0.022(2)	50.40(2)	1
$4f_1$	Tetrahedral	0.139(4)	0.111(3)	48.66(3)	2
2b	Bi-pyramidal	0.142(1)	1.083(1)	39.99(9)	1

[a] IS: isomer shift; QS: quadrupole splitting; H: magnetic hyperfine field. A Lorentzian line width of 0.26 mm s^{-1} resulted from the fit of the spectrum of $BaFe_{12}O_{19}$.

$[Fe_2]_{4f2}[Fe_6]_{12k}[Fe]_{2a}(Fe_2)_{4f1}\{Fe\}_{2b}O_{19}$, where the square brackets, parentheses and curly brackets enclose cations in sites of octahedral, tetrahedral and trigonal bi-pyramidal coordination, respectively. The hexagonal structure of $BaFe_{12}O_{19}$ with the five different Fe nearest-neighbour configurations is shown in Fig. 3.

The mechanically induced evolution of $BaFe_{12}O_{19}$ was followed by XRD. Fig. 4 shows the XRD patterns of the ferrite milled for various times. The XRD pattern of the starting powder is characterized by sharp diffraction peaks corresponding to $BaFe_{12}O_{19}$ with the magnetoplumbite structure and space group $P6_3/mmc$ (JCPDS PDF 27-1029).[9] With increasing milling time, XRD reveals a gradual decrease in the intensity and an associated broadening of the Bragg peaks of the oxide. This reflects a continuous fragmentation of the material accompanied by the refinement of its crystallite size (D) to the nanometer range; with the prolongation of t_m, a monotonous reduction of the average crystallite size of the ferrite to $D = 14$ nm
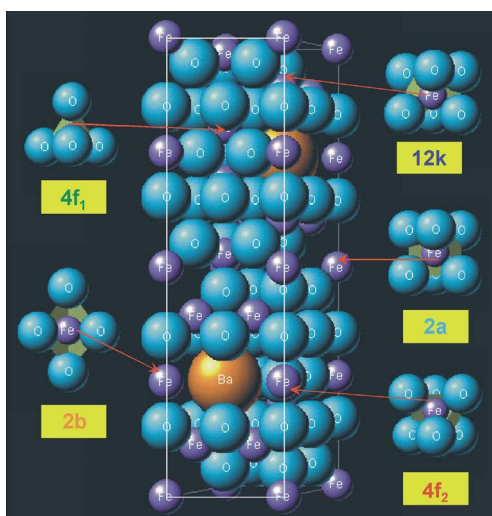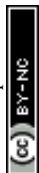

Fig. 3 The crystal structure of the M-type hexaferrite. Fe^{3+} cations are distributed over the sites of octahedral ($4f_2$, 12k, 2a), tetrahedral ($4f_1$) and trigonal bi-pyramidal (2b) coordination.
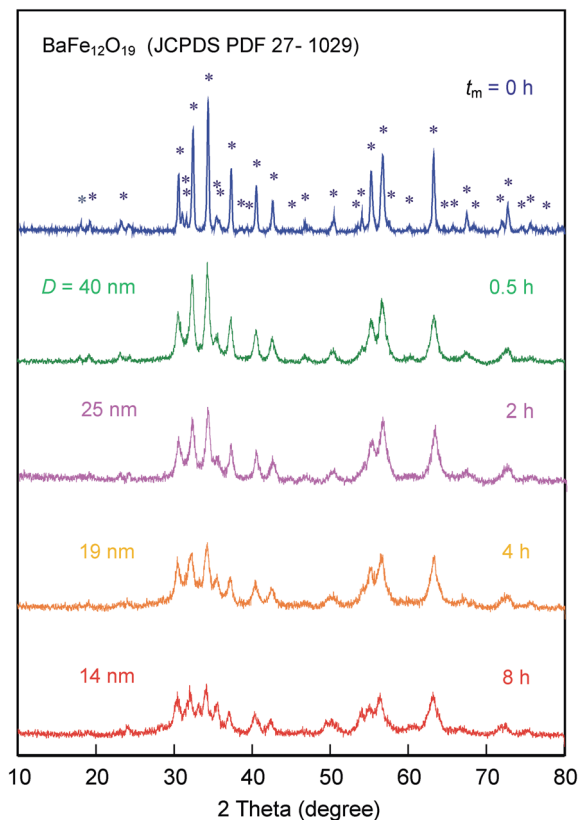
Fig. 4   The XRD patterns of $BaFe_{12}O_{19}$ milled for various milling times. All diffraction peaks of bulk $BaFe_{12}O_{19}$ (denoted by stars) can be indexed to the hexagonal magnetoplumbite structure with the space group $P6_3/mmc$. The milling times (t_m) and the corresponding average crystallite sizes (D) are shown in the figure.

(for $t_m = 8$ h) is observed, see Fig. 4. Simultaneously, the high-energy milling process leads to the formation of a broad diffraction maximum in the range of about 30–40° (2Θ) indicating a partly amorphization of the structure. The superimposition of the relatively broad diffraction reflections of the $BaFe_{12}O_{19}$ phase on a broad diffraction maximum in the range of about 30–40° (2Θ) reflects a typical morphology of the mechanochemically prepared nanostructured oxides[3] consisting of small crystalline regions (often called nanograins or nano-crystallites) surrounded/separated by structurally disordered internal interfaces (grain boundaries) and/or external surfaces (near-surface layers); the detailed TEM analysis of the mechanochemically prepared $BaFe_{12}O_{19}$ nanoparticles is given below. Note that the atomic arrangement in internal interfaces/external surfaces of the mechanically treated materials may lack any long- or short-range order.[3,4] Because of the sensitivity to medium- and long-range structural order, the applied XRD technique loses much of its resolving power in such nanoscale and disordered systems. Therefore, the nature of the mechanically induced structural disorder in $BaFe_{12}O_{19}$ will be analyzed concurrently with the discussion of Mössbauer data (see next paragraph).
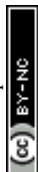
To determine the nature of the mechanically induced structural disorder in $BaFe_{12}O_{19}$, the evolution of its structure on the local atomic scale was followed by ^{57}Fe Mössbauer spectroscopy. The room temperature ^{57}Fe Mössbauer spectra of the material milled for various times are presented in Fig. 5. As can be seen, with increasing t_m, the sextets corresponding to the Fe^{3+} ions located on the five sublattices of the hexaferrite become asymmetric toward the inside of each line, slowly collapse, and are gradually replaced by a broad central doublet with the isomer shift of about 0.21 mm s^{-1} characteristic of Fe^{3+} ions. It should be mentioned in this context that the central doublet is clearly visible after only 30 min of milling (see Fig. 5). Further milling leads to a gradual increase of its relative intensity. After 8 h of mechanical treatment, the sextets disappear completely and the Mössbauer spectrum of the milled $BaFe_{12}O_{19}$ is dominated by the doublet.

The relatively broad shape of the Mössbauer spectral lines for milled $BaFe_{12}O_{19}$, in contrast to the non-treated ferrite, provides clear evidence of a wide distribution of hyperfine interactions experienced by the Fe^{3+} nuclei in the
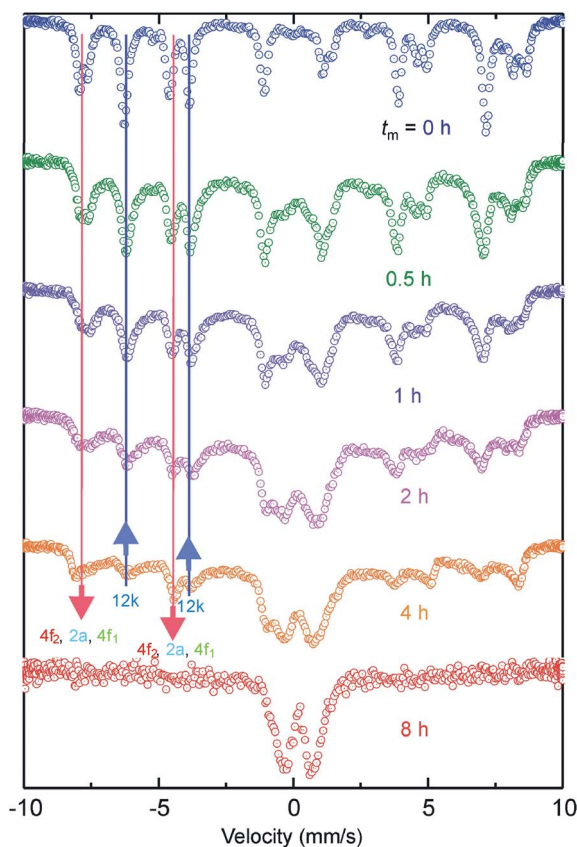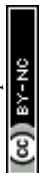

Fig. 5 The room temperature ^{57}Fe Mössbauer spectra of $BaFe_{12}O_{19}$ milled for various milling times (shown in the figure). The arrows emphasize the redistribution of the spectral intensities corresponding to the Fe^{3+} cations in the 4f$_2$, 2a, 4f$_1$ (red arrow) and 12k (blue arrow) crystal sites of the ferrite.

material. This feature may be explained by the presence of a broad distribution of local environments around the Fe nuclei due to the mechanically induced deformation of the constituent polyhedra (FeO_6 octahedra, FeO_4 tetrahedra and FeO_5 triangular bi-pyramids) of the hexaferrite. To elucidate the origin of the broad central doublet in the spectrum of the milled ferrite, we should recall the effect of superparamagnetism.[16] The latter arises if the particle sizes of a material are so small that thermally induced energy fluctuations can overcome the anisotropy energy and change the direction of the magnetization of a particle from one easy axis to another. In line with this, the central doublet in the Mössbauer spectrum of the milled $BaFe_{12}O_{19}$ is related to its particles of such small size that they behave superparamagnetic on the time scale of Mössbauer spectroscopy (about 10^{-9} to 10^{-10} s).[16] Thus, the refinement of the crystallite size of the ferrite results in an increase of the fraction of the superparamagnetic phase at the expense of the ferrimagnetic one; the $BaFe_{12}O_{19}$ sample with the average crystallite size $D = 14$ nm ($t_m = 8$ h) exhibits a pure superparamagnetic behaviour at room temperature.

The important result derived from the present Mössbauer data is that mechanical action on $BaFe_{12}O_{19}$ is accompanied by the changes in the relative intensities of the sublattice subspectra (Fig. 5). It is clearly visible that the relative intensity of the 12k subspectrum (I_{12k}) decreases with increasing milling time; for the bulk $BaFe_{12}O_{19}$, the intensity ratio $I_{12k}/(I_{4f2} + I_{2a} + I_{4f1})$ is 6/5, whereas it takes a value of about 4/5 for the material milled for 4 h. This variation can be explained by a decrease of the population of Fe^{3+} ions on the 12k crystal sites. In this context, it should be noted that similar redistributions of Mössbauer and/or NMR spectral intensities have also been reported for other mechanochemically treated complex oxides, such as spinels,[17] and are consistently explained in terms of the mechanically induced cation redistribution over the available sites of tetrahedral and octahedral coordination provided by the spinel structure. Taking into account that in the magnetoplumbite structure of $BaFe_{12}O_{19}$, in contrast to the spinel structure, all the regular sites are occupied by the cations, the decrease of the intensity ratio $I_{12k}/(I_{4f2} + I_{2a} + I_{4f1})$ from 6/5 to 4/5 can be associated with the mechanically triggered transition of 2 of a total of 6 Fe^{3+} cations (per formula unit of $BaFe_{12}O_{19}$) from the regular 12k sites into the interstitial positions (further denoted by 12k′) of the hexagonal structure. This structural variation has important implications for the macroscopic magnetic properties of the hexaferrite; the detailed discussion of magnetic behaviour of $BaFe_{12}O_{19}$ is given below.

The application of the JSV program[11] enables us to visualize possible 12k′ interstitial sites (cavities) with various radii in the magnetoplumbite structure, where the Fe^{3+} cations could be located. Taking into account the ionic radii of O^{2-}, Fe^{3+}, and Ba^{2+} to be $r_O = 1.24$ Å, $r_{Fe} = 0.785$ Å, and $r_{Ba} = 1.56$ Å, respectively,[18] Fig. 6 illustrates the interstitial sites of various sizes for $BaFe_{12}O_{19}$. The largest cavities in the crystal lattice of the hexaferrite were found to have a radius of $r = 0.881$ Å (Fig. 6a) which is larger than the ionic radius of the Fe^{3+} cations (0.785 Å). This provides evidence that, from the geometrical point of view, the above-mentioned 12k→12k′ structural transition of the Fe^{3+} cations in the hexagonal crystal lattice is generally possible. In this respect, it should be mentioned that the appearance of the Fe^{3+} cations in the interstitial positions of the hexagonal crystal lattice can result in a local distortion of the structure. The latter is supported by
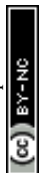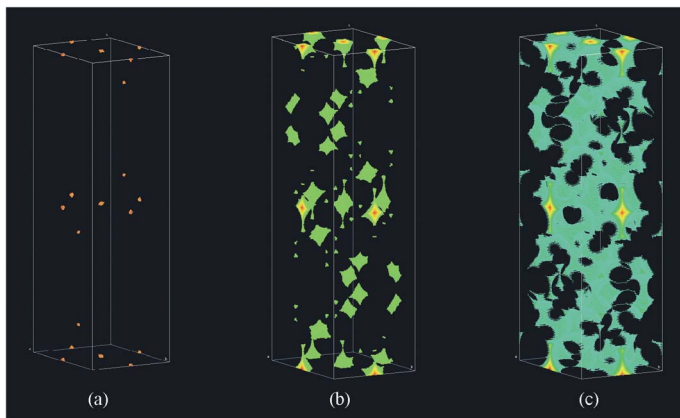
Fig. 6 The visualization of the atomic interstitial sites (cavities) with radii of (a) 0.8, (b) 0.5, and (c) 0.4 Å in the magnetoplumbite structure.

the present Mössbauer study providing clear evidence of a wide distribution of hyperfine interactions experienced by the Fe^{3+} nuclei in the milled hexaferrite due to the distortion of the geometry of its constituent polyhedra (see above). Similar disordering effects, *i.e.*, the nonequilibrium cation distribution and the deformed polyhedron geometry, have already been observed in mechanochemically prepared oxides, such as spinels,[19] olivines[20] and perovskites,[21] as well as ortho-rhombic complex oxides.[22] In the case of mechanosynthesized perovskites (*e.g.*, $BiFeO_3$) and trigonal nanostructured oxides (*e.g.*, $LiNbO_3$), their interface/surface regions have been found to be even amorphous.[21,23] Note that the presence of the amorphous phase in the milled $BaFe_{12}O_{19}$ samples, registered in the present case by XRD and TEM (see below), could be a consequence of a broadly distorted geometry of the constituent polyhedra. Eventually, mechanical action on $BaFe_{12}O_{19}$ can also cause the displacement of the relatively large Ba^{2+} cations from their regular positions leading to additional modifications of the local structure of the ferrite and, finally, to its amorphization.

Representative TEM micrographs of the milled $BaFe_{12}O_{19}$ ($t_m = 8$ h) at low and high magnifications are shown in Fig. 7. It is revealed that the milled material consists of nanoparticles with a size distribution ranging from about 8 to 20 nm, which consistent with the average crystallite size determined by XRD. The nanoparticles are found to be roughly spherical. An interesting observation is that the amorphous phase, evidenced by XRD, is confined to the near-surface layers/interfaces of the $BaFe_{12}O_{19}$ nanoparticles. As clearly seen, the milled hexaferrite consists of crystalline regions, represented by lattice fringes in Fig. 7b, and amorphous rim regions with the thickness of about 2 nm. Based on the present high-resolution TEM observations as well as on the analogy with previous work on mechanochemically prepared complex nanooxides,[3] we can state that a far-from-equilibrium distribution of the Fe^{3+} cations in the milled $BaFe_{12}O_{19}$, its deformed polyhedra, and the amorphous phase, evidenced by Mössbauer spectroscopy and XRD, respectively, are confined to the particle's near-surface layers with the thickness extending up to about 2 nm. The shell thickness in the milled $BaFe_{12}O_{19}$ nanoparticles is comparable to that observed for other nanooxides
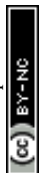
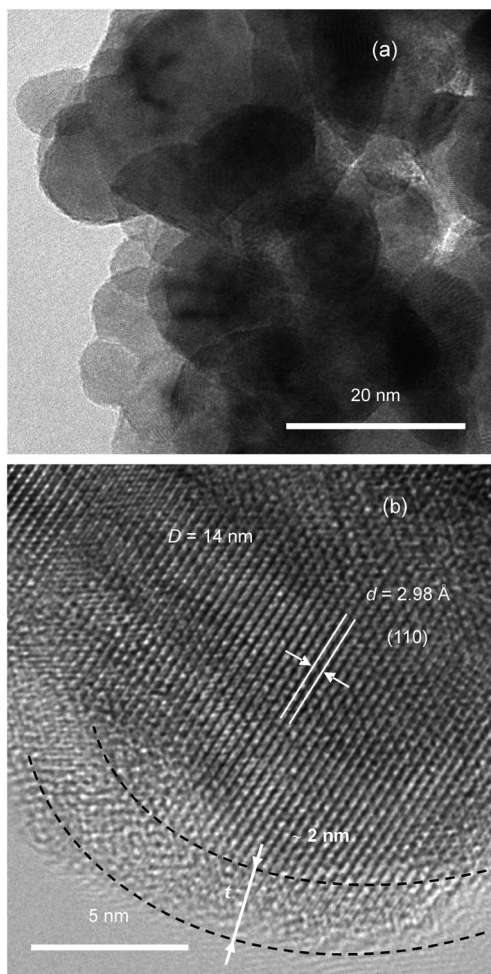**Fig. 7** (a) Bright-field and (b) high-resolution TEM images of the nanocrystalline $BaFe_{12}O_{19}$ prepared by high-energy milling of the corresponding bulk material. The high-resolution TEM micrograph demonstrates the inhomogeneous structure of the produced nanoparticles with the average size $D = 14$ nm which exhibit a clearly defined rim region and a core region. The so-called core–shell configuration of the nanoparticles with the thickness t of the surface shell of about 2 nm is evident. The lattice fringes correspond to the crystallographic plane (110) ($d = 2.98$ Å) of the $BaFe_{12}O_{19}$ phase (JCPDS PDF 27-1029).

prepared by mechanochemical routes. We note that, in general, up to 2 nm is a typical thickness of the grain boundary/surface shell regions in nanostructured mechanochemically prepared oxides.[3,4]

Assuming a spherical shape of $BaFe_{12}O_{19}$ nanoparticles and taking both their average diameter ($D = 14$ nm) and the thickness of their surface shell ($t = 2$ nm) as determined experimentally by XRD and TEM, respectively, one can easily deduce quantitative information on the volume fraction of disordered surface shell
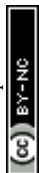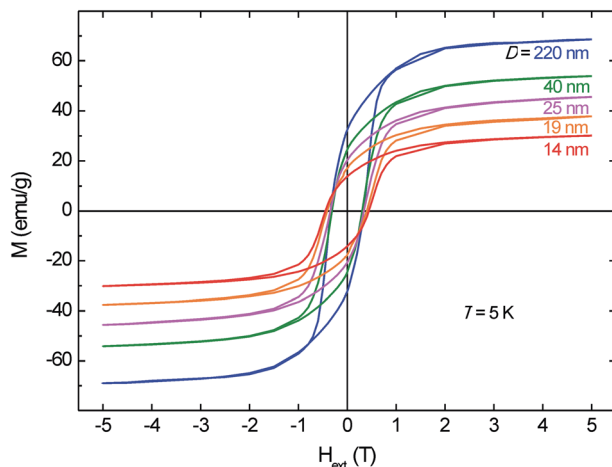
Fig. 8 Magnetization hysteresis loops for bulk and nanoscale mechanically treated BaFe$_{12}$O$_{19}$. Hysteresis loops were measured at 5 K after field cooling with H_{ext} = 5 T. The average crystallite sizes of the BaFe$_{12}$O$_{19}$ samples are shown in the figure.

regions, w, to the volume of whole particles ($w = V_{shell}/(V_{core} + V_{shell})$) in the nanomaterial.‡ The estimated value of $w \approx 0.636$ indicates that about 64% of atoms in the milled ferrite are in a structurally disordered state located in the surface shell of nanoparticles. In this context, it should be noted that nano-materials, in general, and especially those prepared by mechanochemical pro-cessing exhibit a high volume fraction of structurally disordered regions.[3,4]

The far-from-equilibrium structural state, confined to the particle's near-surface layers of the mechanically treated ferrite, has significant implications for its magnetism. Fig. 8 compares the hysteresis loops measured at 5 K for bulk and milled BaFe$_{12}$O$_{19}$. An interesting observation is that the saturation magnetization (M_{sat}) of the ferrite decreases with increasing t_m (*i.e.*, with decreasing D). By extrapolating the high-field region ($H_{ext} > 3.5$ T) of the $M(H_{ext})$ curves to infinite field, we estimated the M_{sat} values of hexaferrites with various particle sizes, see Table 2. They span over a wide interval from M_{sat} = 68.601(1) emu g^{-1} (for bulk BaFe$_{12}$O$_{19}$) to M_{sat} = 30.093(6) emu g^{-1} (for nano-BaFe$_{12}$O$_{19}$ with D = 14 nm). Another feature observed is that the nanoscale BaFe$_{12}$O$_{19}$ exhibits an enhanced magnetic hardness, *i.e.*, the coercive field of the nanomaterial (H_c = 0.449(5) T) is about 34% larger than that of the bulk material (H_c = 0.334(3) T), see Table 2. Obviously, these large variations in magnetization and coercivity offer an ample opportunity to manipulate and tailor the functional properties of this magneti-cally hard material.

The information on the nonequilibrium distribution of the Fe^{3+} cations and the distorted polyhedron geometry in the milled BaFe$_{12}$O$_{19}$, obtained from the analysis of Mössbauer data, is very helpful in the interpretation of its reduced magnetization. Because Ba^{2+} ions possess no magnetic moment, the total magnetic moment μ of BaFe$_{12}$O$_{19}$ is entirely due to the uncompensated magnetic

---

‡ $w = [1 - (1 - 2t/D)^3]$.
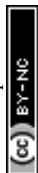
Faraday Discussions

Table 2 Average crystallite size (D), saturation magnetization (M_{sat}), coercive field (H_c), and remanent magnetization (M_r) derived from the hysteresis loops measured at 5 K for $BaFe_{12}O_{19}$ milled for various times (t_m)[a]
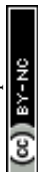
t_m (h)	D (nm)	M_{sat} (emu g^{-1})	H_c (T)	M_r (emu g^{-1})
0	220	68.601(1)	0.334(3)	32.433(8)
0.5	40	54.021(1)	0.312(2)	24.513(2)
2	25	45.610(2)	0.344(4)	20.246(9)
4	19	37.902(2)	0.411(8)	16.972(9)
8	14	30.093(6)	0.449(5)	13.706(5)

[a] Values of the saturation magnetization are obtained by linear extrapolation of the high-field region ($H_{ext} > 3.5$ T) of the $M(1/H_{ext})$ curves to infinite field.

moments of the ferric ions. Thus, based on the structural formula of bulk $BaFe_{12}O_{19}$ emphasizing its spin arrangement, $Ba[Fe_2\downarrow]_{4f2}[Fe_6\uparrow]_{12k}[Fe\uparrow]_{2a}(Fe_2\downarrow)_{4f1}\{Fe\uparrow\}_{2b}O_{19}$, we can calculate the effective magnetic moment (per formula unit) of the hexaferrite as $(-2 + 6 + 1 - 2 + 1) \times \mu_{Fe} = 20\ \mu_B$, where μ_{Fe} is the magnetic moment of the Fe^{3+} ion; $\mu_{Fe} = 5\ \mu_B$ (μ_B is Bohr magneton (see also Table 3). On the other hand, taking into account the mechanically triggered transition of 2 of a total of 6 Fe^{3+} cations from the regular 12k octahedral sites into the interstitial 12k$'$ positions, the effective magnetic moment of the milled hexaferrite can be expressed as $\mu = (-2 + 4 + 1 - 2 + 1) \times \mu_{Fe} = 10\ \mu_B/f.u.$ (the calculation was made under the assumption that the spins of the Fe^{3+} cations in the interstitial sites are randomly aligned, resulting in zero net magnetic moment). Thus, the cation disorder in $BaFe_{12}O_{19}$ generally tends to reduce its magnetic moment. However, it should be noted that the presence of nonequilibrium cation distribution and/or distorted polyhedron geometry in ferrites effects their spin alignments on all available sublattices leading to the formation of canted spin arrangements as it was demonstrated for mechanochemnically prepared magnetic spinels and perovskites.[3] Thus, a more realistic picture of the milled $BaFe_{12}O_{19}$ is that the magnetic moment of each sublattice is affected by spin canting. Moreover, the confinement of the structural disorder to the

Table 3 The calculated effective magnetic moment (μ) per formula unit of bulk and nanocrystalline $BaFe_{12}O_{19}$ materials

Material	Site	Number of Fe^{3+} ions/f.u.	Spin orientation	μ per f.u.
Bulk $BaFe_{12}O_{19}$ ($t_m = 0$ h, $D = 220$ nm)	$4f_2$	2	$\downarrow$	$(-2 + 6 + 1 - 2 + 1) \times$
	12k	6	$\uparrow$	$5\ \mu_B = = 20\ \mu_B$
	2a	1	$\uparrow$	
	$4f_1$	2	$\downarrow$	
	2b	1	$\uparrow$	
Nanocrystalline $BaFe_{12}O_{19}$ ($t_m = 4$ h, $D = 19$ nm)	$4f_2$	2	$\downarrow$	$(-2 + 4 + 1 - 2 + 1) \times$
	12k	4	$\uparrow$	$5\ \mu_B = = 10\ \mu_B$
	12k$'$	2	random	
	2a	1	$\uparrow$	
	$4f_1$	2	$\downarrow$	
	2b	1	$\uparrow$	

particle's interfaces/near-surface layers can even results in the formation of magnetically inactive (the so-called "dead") regions with zero net magnetic moment.[24]

In the following, we will estimate the shell thickness using the experimentally determined D and M_{sat} values of $BaFe_{12}O_{19}$ milled for various times (see Table 2). Assuming that t is independent of D and that the shell is magnetically "dead" ($M_{shell} = 0$), the variation of M_{sat} with D will then be described by

$$M_{sat}^{1/3} = M_{core}^{1/3}(1 - 2t/D),$$

where M_{core} is the saturation magnetization of the core of nanoparticles.[24] As can be seen in Fig. 9, the present experimental data $M_{sat}^{1/3}$ and $1/D$ indeed show a good linear relationship. Note that the intercept at $1/D = 0$ and the slope of the straight line correspond to $M_{core}^{1/3}$ and $2tM_{core}^{1/3}$, respectively. From a linear fit to the data points, the saturation magnetization of the particle core and the thickness of the shell were estimated to be $M_{core} \approx 71.7$ emu g^{-1} and $t \approx 1.8$ nm, respectively. The value of M_{core} thus obtained is close to the saturation magnetization measured for bulk $BaFe_{12}O_{19}$, 68.6 emu g^{-1}. The value of the shell thickness obtained is in reasonable agreement with that estimated directly from high-resolution TEM experiments (2 nm). Based on this agreement, we can state that the magnetism of the milled $BaFe_{12}O_{19}$ is controlled by the mechanically induced far-from-equilibrium structural disorder, which is confined to the interface/surface regions of the nanoferrite.

Conclusions

The structural and magnetic evolution of $BaFe_{12}O_{19}$ caused by high-energy milling has been studied. During the milling process, the material is subjected to a continuous fragmentation accompanied by the reduction of its crystallite size to the 8–20 nm size range. In addition to the XRD method being sensitive to
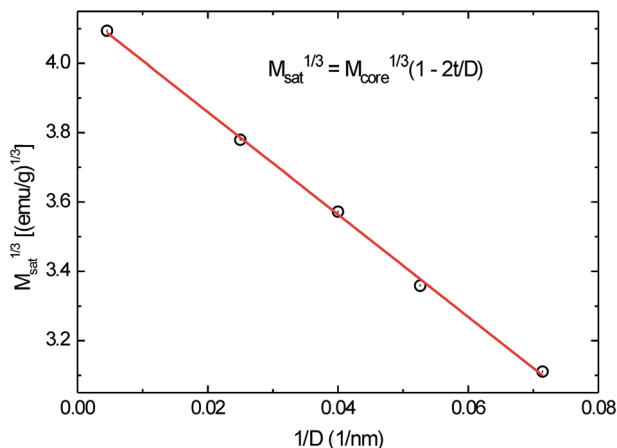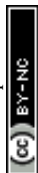

Fig. 9 $M_{sat}^{1/3}$ vs $1/D$ plot, where M_{sat} is the saturation magnetization and D is the diameter of the $BaFe_{12}O_{19}$ nanoparticles.

medium- and long-range structural order, the mechanically induced evolution of $BaFe_{12}O_{19}$ was followed by ^{57}Fe Mössbauer spectroscopy, which made possible observations on a local atomic scale. The latter method revealed the presence of a broad distribution of local environments around the Fe^{3+} cations in the nano-ferrite due to the mechanically induced deformation of its constituent polyhedra (FeO_6 octahedra, FeO_4 tetrahedra and FeO_5 triangular bi-pyramids). The response of $BaFe_{12}O_{19}$ to mechanical action is found to be accompanied by the mechanically triggered transition of Fe^{3+} cations from the regular 12k octahedral sites into the interstitial positions of the hexagonal structure. The refinement of the crystallite size of the ferrite results in an increase of the fraction of the super-paramagnetic phase at the expense of the ferrimagnetic one; the $BaFe_{12}O_{19}$ sample with the average crystallite size of about 14 nm exhibits a pure super-paramagnetic behaviour at room temperature. The as-prepared nanoparticles are found to be roughly spherical, consisting of a crystalline inner core surrounded/separated by an amorphous surface shell/interface region with the thickness and the volume fraction extending up to about 2 nm and 64%, respectively. The far-from-equilibrium structural state, confined to the particle's near-surface layers of the mechanically treated ferrite, has significant implications for its magnetism. It is found that the saturation magnetization of $BaFe_{12}O_{19}$ decreases with decreasing particle size from about 69 emu g^{-1} (for bulk $BaFe_{12}O_{19}$) to about 30 emu g^{-1} (for nanoferrite with $D = 14$ nm). On the other hand, the coercive field of the nanomaterial is about 34% larger than that of the bulk sample. The macroscopic magnetic behaviour of the milled $BaFe_{12}O_{19}$ is attributed to the effects of the mechanically induced far-from-equilibrium structural disorder, which is located in the interface/surface regions of the nanoferrite.

Acknowledgements

Notes and references

1 *Mechanochemistry*, ed. S. L. James and T. Friščić, *Chem. Soc. Rev.*, 2013, **42**, 7487–7740.

2 *Mechanoresponsive Materials*, ed. C. Weder, *J. Mater. Chem.*, 2011, **21**, 8217–8476.

3 V. Šepelák, A. Düvel, M. Wilkening, K.-D. Becker and P. Heitjans, *Chem. Soc. Rev.*, 2013, **42**, 7507.

4 V. Šepelák, S. Bégin-Colin and G. Le Caër, *Dalton Trans.*, 2012, **41**, 11927.

5 S. J. Campbell, E. Wu, W. A. Kaczmarek and K. D. Jayasuriya, *Hyperfine Interact.*, 1994, **92**, 933.

6 K. Haneda and H. Kojima, *J. Am. Ceram. Soc.*, 1973, **57**, 68.

7 G. Tan and X. Chen, *J. Magn. Magn. Mater.*, 2013, **327**, 87.

8 D. Belušova, T. Alshuth, R. H. Schuster, M. Myndyk, V. Šepelák and I. Hudec, *Kaut. Gummi Kunstst.*, 2008, **3**, 118.
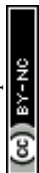
9 Joint Committee on Powder Diffraction, *Standards (JCPDS) Powder Diffraction File (PDF)*, International Centre for Diffraction Data, Newtown Square, PA, 2004.

10 K. Brandenburg and H. Putz, *Diamond – Crystal and Molecular Structure Visualization Software, Version 3.0a*, Crystal Impact GbR, Bonn, Germany, 2004.

11 S. Weber, *J. Appl. Crystallogr.*, 1999, **32**, 1027; S. Weber, *Java Structure Viewer (JSV), 1.08lite*, 1999.

12 K. Lagarec and D. G. Rancourt, *Recoil – Mössbauer Spectral Analysis Software for Windows, Version 1.02*, Department of Physics, University of Ottawa, Ottawa, ON, 1998.

13 V. Šepelák and K. D. Becker, *J. Mater. Synth. Process.*, 2000, **8**, 155.

14 F.-M. Gao, D.-C. Li and S.-Y. Zhang, *J. Phys.: Condens. Matter*, 2003, **15**, 5079.

15 F. Menil, *J. Phys. Chem. Solids*, 1985, **46**, 763.

16 G. J. Long, *Mössbauer Spectroscopy Applied to Inorganic Chemistry*, Plenum Press, New York, 1987, vol. 2.

17 V. Šepelák, I. Bergmann, S. Indris, A. Feldhoff, H. Hahn, K. D. Becker, C. P. Grey and P. Heitjans, *J. Mater. Chem.*, 2011, **21**, 8332; V. Šepelák, D. Baabe, D. Mienert, D. Schultze, F. Krumeich, F. J. Litterst and K. D. Becker, *J. Magn. Magn. Mater.*, 2003, **257**, 377; V. Šepelák, D. Baabe, F. J. Litterst and K. D. Becker, *J. Appl. Phys.*, 2000, **88**, 5884; V. Šepelák, D. Baabe and K. D. Becker, *J. Mater. Synth. Process.*, 2000, **8**, 333; P. Druska, U. Steinike and V. Šepelák, *J. Solid State Chem.*, 1999, **146**, 13; V. Šepelák, K. Tkáčová, V. V. Boldyrev, S. Wißmann and K. D. Becker, *Phys. B*, 1997, **234–236**, 617.

18 R. D. Shannon, *Acta Crystallogr., Sect. A: Cryst. Phys., Diffr., Theor. Gen. Crystallogr.*, 1976, **32**, 751.

19 V. Šepelák, A. Feldhoff, P. Heitjans, F. Krumeich, D. Menzel, F. J. Litterst, I. Bergmann and K. D. Becker, *Chem. Mater.*, 2006, **18**, 3057; V. Šepelák, S. M. Becker, I. Bergmann, S. Indris, M. Scheuermann, A. Feldhoff, C. Kübel, M. Bruns, N. Stürzl, A. S. Ulrich, M. Ghafari, H. Hahn, C. P. Grey, K. D. Becker and P. Heitjans, *J. Mater. Chem.*, 2012, **22**, 3117.

20 V. Šepelák, M. Myndyk, M. Fabián, K. L. Da Silva, A. Feldhoff, D. Menzel, M. Ghafari, H. Hahn, P. Heitjans and K. D. Becker, *Chem. Commun.*, 2012, **48**, 11121.

21 K. L. Da Silva, D. Menzel, A. Feldhoff, C. Kübel, M. Bruns, A. Paesano, Jr, A. Düvel, M. Wilkening, M. Ghafari, H. Hahn, F. J. Litterst, P. Heitjans, K. D. Becker and V. Šepelák, *J. Phys. Chem. C*, 2011, **115**, 7209.

22 L. J. Berchmans, M. Myndyk, K. L. Da Silva, A. Feldhoff, J. Šubrt, P. Heitjans, K. D. Becker and V. Šepelák, *J. Alloys Compd.*, 2010, **500**, 68; V. Šepelák, K. D. Becker, I. Bergmann, S. Suzuki, S. Indris, A. Feldhoff, P. Heitjans and C. P. Grey, *Chem. Mater.*, 2009, **21**, 2518.

23 P. Heitjans and M. Wilkening, *MRS Bull.*, 2009, **34**, 915.

24 V. Šepelák, I. Bergmann, A. Feldhoff, P. Heitjans, F. Krumeich, D. Menzel, F. J. Litterst, S. J. Campbell and K. D. Becker, *J. Phys. Chem. C*, 2007, **111**, 5026.